

A PHENOMENOLOGICAL 3D MODEL DESCRIBING STRESS-INDUCED SOLID PHASE TRANSFORMATIONS WITH PERMANENT INELASTICITY

F. AURICCHIO^{a,b}, A. REALI^{a*} and U. STEFANELLI^b

^a *Dipartimento di Meccanica Strutturale, Università degli Studi di Pavia,
via Ferrata 1, 27100, Pavia, Italy*

**E-mail: alessandro.reali@unipv.it*

^b *Istituto di Matematica Applicata e Tecnologie Informatiche
via Ferrata 1, 27100, Pavia, Italy*

The diffusion and the use of shape memory alloys in many aeronautical, biomedical and structural engineering applications is resulting in an increasing research effort toward a reliable and complete modeling of their macroscopic behaviour. As many models for SMA available in the literature consider fully reversible phase transformations (i.e. no permanent inelastic strains), which are proved by experiments to be sometimes a not fully realistic approximation, we present here a 3D model capable of including permanent inelastic effects combined with a good description of pseudo-elastic and shape-memory behaviours. We also show numerical results from both uniaxial and non-proportional biaxial tests, which aim at assessing model features and performance.

Keywords: Shape memory alloys; Permanent inelasticity; Phase transformation; Pseudo-elasticity; Shape-memory effect; Non-proportional biaxial tests.

1. Introduction

The great and always increasing interest in SMA materials (cf. Refs. 1,2.) and their industrial applications is deeply stimulating the research on constitutive laws. As a consequence, many models able to reproduce one or both of the well-known SMA macroscopic behaviours, referred to as *pseudo-elasticity* and *shape-memory effect*, have been recently proposed in the literature (see for instance Refs. 3–11).

In particular, the constitutive law proposed in Ref. 12 and improved in Ref. 13 seems to be attractive. Developed within the theory of irreversible thermodynamics, this model is in fact able to describe both pseudo-elasticity and shape-memory effect and the corresponding solution algo-

rithm, based on a plasticity-like return map procedure, is simple and robust.

However, we have to stress that most of the SMA models present in the literature are not able to reproduce other experimentally observed SMA behaviours such as permanent inelasticity and degradation effects, as shown by Fig. 1 (Ref. 14). In fact, such a figure presents pseudo-elastic loops showing an increasing level of permanent inelasticity that saturates on a stable value after a certain number of cycles. The same figure highlights that degradation effects should be taken into account as well. For a description of these behaviours from a physical point of view the interested reader is referred to classical SMA textbooks such as Refs. 15,16. Moving from these experimental evidences, some models accounting for permanent inelastic effects have been recently proposed in the literature (see e.g. Refs. 17–20).

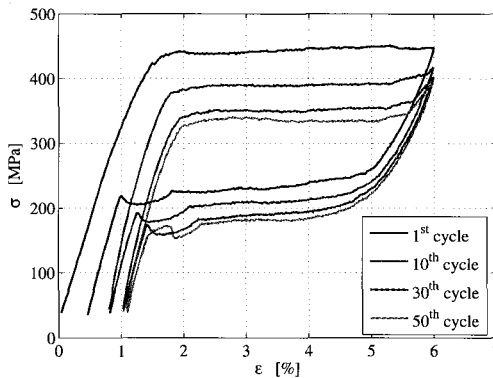


Fig. 1. Experimental results on a SMA Ni-Ti wire. Cyclic tension test: stress versus strain up to 6% strain.

In particular, in this work we discuss a phenomenological constitutive model, able to reproduce pseudo-elastic and shape-memory behaviours as well as to include permanent inelasticity and degradation effects, which has been introduced in Ref. 21,22. The model consists of an extension of the model discussed in Ref. 13, by means of the introduction of a new internal variable describing permanent inelastic strains. In the following, an analytic description of the constitutive equations is presented together with numerical experiments which show main features and performance of the model.

2. 3D phenomenological model for stress-induced solid phase transformation with permanent inelasticity

2.1. Time-continuous frame

The model assumes the total strain $\boldsymbol{\varepsilon}$ and the absolute temperature T as control variables, the transformation strain \mathbf{e}^{tr} and the permanent inelastic strain \mathbf{q} as internal ones. As in Ref. 13, the second-order tensor \mathbf{e}^{tr} describes the strain associated to the transformation between the two solid phases referred to as martensite and austenite. Here, this quantity has no fully reversible evolution and the permanent inelastic strain \mathbf{q} gives a measure of the part of \mathbf{e}^{tr} that cannot be recovered when unloading to a zero stress state. Moreover, we require that

$$\|\mathbf{e}^{tr}\| \leq \varepsilon_L, \quad (1)$$

where $\|\cdot\|$ is the usual Euclidean norm and ε_L is a material parameter corresponding to the maximum transformation strain reached at the end of the transformation during an uniaxial test.

Assuming a small strain regime, justified by the fact that the approximation of large displacements and small strains is valid for several applications, the following standard additive decomposition can be considered

$$\boldsymbol{\varepsilon} = \frac{\theta}{3} \mathbf{1} + \mathbf{e},$$

where $\theta = \text{tr}(\boldsymbol{\varepsilon})$ and \mathbf{e} are respectively the volumetric and the deviatoric part of the total strain $\boldsymbol{\varepsilon}$, while $\mathbf{1}$ is the second-order identity tensor. The free energy density function Ψ for a polycrystalline SMA material is then expressed as the convex potential

$$\begin{aligned} \Psi(\theta, \mathbf{e}, T, \mathbf{e}^{tr}, \mathbf{q}) = & \frac{1}{2} K \theta^2 + G \|\mathbf{e} - \mathbf{e}^{tr}\|^2 + \beta \langle T - M_f \rangle \|\mathbf{e}^{tr} - \mathbf{q}\| \\ & + \frac{1}{2} h \|\mathbf{e}^{tr}\|^2 + \frac{1}{2} H \|\mathbf{q}\|^2 - A \mathbf{e}^{tr} : \mathbf{q} + \mathcal{I}_{\varepsilon_L}(\mathbf{e}^{tr}), \end{aligned} \quad (2)$$

where K and G are respectively the bulk and the shear modulus, β is a material parameter related to the dependence of the critical stress on the temperature, M_f is the temperature below which only martensite phase is stable, h defines the hardening of the phase transformation, H controls the saturation of the permanent inelastic strain evolution, and A controls the degradation of the model. Moreover, we make use of the indicator function

$$\mathcal{I}_{\varepsilon_L}(\mathbf{e}^{tr}) = \begin{cases} 0 & \text{if } \|\mathbf{e}^{tr}\| \leq \varepsilon_L \\ +\infty & \text{otherwise,} \end{cases}$$

in order to satisfy the transformation strain constraint (1); we also introduce the positive part function $\langle \cdot \rangle$, defined as

$$\langle a \rangle = \begin{cases} a & \text{if } a > 0 \\ 0 & \text{otherwise.} \end{cases}$$

We remark that in the expression of the free energy we neglect the contributions due to thermal expansion and change in temperature with respect to the reference state, since we are not interested here in a complete description of the thermomechanical coupled problem. However, the interested reader may find in Refs. 13,23 how it is possible to take into account these aspects in the formulation. We also stress that, due to the fact that we do not consider a fully thermomechanical coupled model, Ψ should be more properly referred to as a temperature-parameterized free energy density function.

Moreover, since we use only a single internal variable second-order tensor to describe phase transformations, at most it is possible to distinguish between a generic parent phase (not associated to any macroscopic strain) and a generic product phase (associated to a macroscopic strain), as in Ref. 13. Accordingly, the model does not distinguish between the austenite and the twinned martensite, as both these phases do not produce macroscopic strain.

We furthermore highlight that, for the sake of simplicity, the present model does not reflect the difference existing between the austenite and the martensite elastic properties.

Starting from the free energy function Ψ and following standard arguments, we can derive the constitutive equations

$$\left\{ \begin{array}{l} p = \frac{\partial \Psi}{\partial \theta} = K\theta, \\ s = \frac{\partial \Psi}{\partial \mathbf{e}} = 2G(\mathbf{e} - \mathbf{e}^{tr}), \\ \eta = -\frac{\partial \Psi}{\partial T} = -\beta \|\mathbf{e}^{tr} - \mathbf{q}\| \frac{\langle T - M_f \rangle}{|T - M_f|}, \\ \mathbf{X} = -\frac{\partial \Psi}{\partial \mathbf{e}^{tr}} = \mathbf{s} - \beta \langle T - M_f \rangle \frac{\mathbf{e}^{tr} - \mathbf{q}}{\|\mathbf{e}^{tr} - \mathbf{q}\|} - h\mathbf{e}^{tr} + A\mathbf{q} - \gamma \frac{\mathbf{e}^{tr}}{\|\mathbf{e}^{tr}\|}, \\ \mathbf{Q} = -\frac{\partial \Psi}{\partial \mathbf{q}} = \beta \langle T - M_f \rangle \frac{\mathbf{e}^{tr} - \mathbf{q}}{\|\mathbf{e}^{tr} - \mathbf{q}\|} - H\mathbf{q} + A\mathbf{e}^{tr}, \end{array} \right. \quad (3)$$

where $p = \text{tr}(\boldsymbol{\sigma})/3$ and \mathbf{s} are respectively the volumetric and the deviatoric part of the stress $\boldsymbol{\sigma}$, \mathbf{X} is a thermodynamic stress-like quantity associated to the transformation strain \mathbf{e}^{tr} , \mathbf{Q} is a thermodynamic stress-like quantity

associated to the permanent inelastic strain \mathbf{q} , and η is the entropy. The variable γ results from the indicator function subdifferential $\partial\mathcal{I}_{\varepsilon_L}(\mathbf{e}^{tr})$ and it is defined as

$$\begin{cases} \gamma = 0 & \text{if } \|\mathbf{e}^{tr}\| < \varepsilon_L, \\ \gamma \geq 0 & \text{if } \|\mathbf{e}^{tr}\| = \varepsilon_L, \end{cases}$$

so that $\partial\mathcal{I}_{\varepsilon_L}(\mathbf{e}^{tr}) = \gamma \frac{\mathbf{e}^{tr}}{\|\mathbf{e}^{tr}\|}$.

To describe phase transformation and inelasticity evolution, we choose (following a plasticity-like terminology) a limit function F defined as

$$F(\mathbf{X}, \mathbf{Q}) = \|\mathbf{X}\| + \kappa\|\mathbf{Q}\| - R, \quad (4)$$

where κ is a material parameter defining a scaling modulus between the inelastic effect and the phase transformation, while R is the radius of the elastic domain. We stress that, in order to reproduce the asymmetric behaviour in tension and compression shown by SMA in many experiments, different and more complicate choices for F should be introduced in (4), as it is done in Ref. 13 where a Prager-Lode type limit function is employed.

Considering an associative framework, the flow rules for the internal variables take the form

$$\begin{cases} \dot{\mathbf{e}}^{tr} = \dot{\zeta} \frac{\partial F}{\partial \mathbf{X}} = \dot{\zeta} \frac{\mathbf{X}}{\|\mathbf{X}\|}, \\ \dot{\mathbf{q}} = \dot{\zeta} \frac{\partial F}{\partial \mathbf{Q}} = \dot{\zeta} \kappa \frac{\mathbf{Q}}{\|\mathbf{Q}\|}. \end{cases} \quad (5)$$

The model is finally completed by the classical Kuhn-Tucker conditions

$$\begin{cases} \dot{\zeta} \geq 0, \\ F \leq 0, \\ \dot{\zeta} F = 0. \end{cases} \quad (6)$$

3. Time-discrete frame

Let us now focus on the crucial issue of computing the stress and internal variable evolution of a SMA sample in a strain-driven situation. We shall directly concentrate ourselves on the solution of the time-incremental problem. Namely, we discretize the time-interval of interest $[0, t_f]$ by means of the partition $I = \{0 = t_0 < t_1 < \dots < t_{N-1} < t_n = t_f\}$, assume to be given the state of the system $(p_n, \mathbf{s}_n, \eta_n, \mathbf{e}_n^{tr}, \mathbf{q}_n)$ at time t_n , the actual total strain (θ, \mathbf{e}) and temperature T at time t_{n+1} (note that for notation simplicity here and in the following we drop the subindex $n + 1$ for all the

variables computed at time t_{n+1}), and solve for (p, s, η, e^{tr}, q) . For the sake of numerical convenience, instead of solving (3) we prefer to perform some regularization. Indeed, we let $\|\cdot\|$ be defined as

$$\|\mathbf{a}\| = \sqrt{\|\mathbf{a}\|^2 + \delta} - \sqrt{\delta},$$

(δ is a user-defined parameter controlling the smoothness of the norm regularization) and introduce the regularized free energy density $\bar{\Psi}$ and limit function \bar{F} as

$$\begin{aligned} \bar{\Psi}(\theta, \mathbf{e}, T, e^{tr}, \mathbf{q}) &= \frac{1}{2}K\theta^2 + G\|\mathbf{e} - e^{tr}\|^2 + \beta(T - M_f)\overline{\|\mathbf{e}^{tr} - \mathbf{q}\|} \\ &\quad + \frac{1}{2}h\|e^{tr}\|^2 + \frac{1}{2}H\|\mathbf{q}\|^2 - Ae^{tr} : \mathbf{q} + \mathcal{I}_{\varepsilon_L}(e^{tr}), \end{aligned} \quad (7)$$

$$\bar{F}(\mathbf{X}, \mathbf{Q}) = \|\mathbf{X}\| + \kappa\overline{\|\mathbf{Q}\|} - R, \quad (8)$$

Finally, the updated values $(p, s, \eta, e^{tr}, \mathbf{q})$ for regularized constitutive model can be computed from the following relations

$$\left\{ \begin{array}{l} p = K\theta, \\ s = 2G(\mathbf{e} - e^{tr}), \\ \eta = -\beta\overline{\|\mathbf{e}^{tr} - \mathbf{q}\|} \frac{\langle T - M_f \rangle}{|T - M_f|}, \\ \mathbf{X} = s - \beta(T - M_f) \frac{e^{tr} - \mathbf{q}}{\sqrt{\|\mathbf{e}^{tr} - \mathbf{q}\|^2 + \delta}} - h e^{tr} + A\mathbf{q} - \gamma \frac{e^{tr}}{\|e^{tr}\|}, \\ \mathbf{Q} = \beta(T - M_f) \frac{e^{tr} - \mathbf{q}}{\sqrt{\|\mathbf{e}^{tr} - \mathbf{q}\|^2 + \delta}} - H\mathbf{q} + Ae^{tr}, \\ e^{tr} = e_n^{tr} + \Delta\zeta \frac{\mathbf{X}}{\|\mathbf{X}\|}, \\ \mathbf{q} = \mathbf{q}_n + \Delta\zeta \kappa \frac{\mathbf{Q}}{\sqrt{\|\mathbf{Q}\|^2 + \delta}}, \\ \bar{F} = \|\mathbf{X}\| + \kappa\overline{\|\mathbf{Q}\|} - R, \end{array} \right. \quad (9)$$

along with the requirements

$$\left\{ \begin{array}{l} \gamma \geq 0, \\ \|e^{tr}\| \leq \varepsilon_L, \\ \Delta\zeta \geq 0, \quad \bar{F} \leq 0, \quad \Delta\zeta\bar{F} = 0, \end{array} \right. \quad (10)$$

where $\Delta\zeta = \zeta - \zeta_n = \int_{t_n}^{t_{n+1}} \dot{\zeta} dt$ is the time-integrated consistency parameter.

We shall clearly state that our numerical experiments are not performed on the model of Sec. 2 but rather on its above-introduced δ -regularized version. This choice turns out to be quite convenient from the numerical

viewpoint and preserves most of the characteristic features of the model. Moreover, it can be proved that the δ -regularized model converges to the original one as the regularization parameter δ goes to 0. This fact along with additional mathematical analysis of the model are the subject of the forthcoming contribution Ref. 24 (see also Ref. 25 for similar problems).

3.1. Solution algorithm

The solution of the discrete model is performed by means of an elastic-predictor inelastic-corrector return map procedure as in classical plasticity problems (cf. Ref. 26). An elastic trial state is evaluated keeping frozen the internal variables, then a trial value of the limit function is computed to verify the admissibility of the trial state. If this is not verified, the step is inelastic and the evolution equations have to be integrated.

We remark that, as in Ref. 13, we distinguish two inelastic phases in our model: a non-saturated phase ($\|e^{tr}\| < \varepsilon_L, \gamma = 0$) and a saturated one ($\|e^{tr}\| = \varepsilon_L, \gamma \geq 0$). In our solution procedure we start assuming to be in a non-saturated phase, and when convergence is attained we check if our assumption is violated. If the non-saturated solution is not admissible, we search for a new solution considering saturated conditions.

For each inelastic step, we have to solve the nonlinear system constituted by equations (9). As the aim of this paper is to show the model behaviour without focusing on algorithmic problems, we find a solution to the nonlinear system by means of the function *fsolve* implemented in the optimization toolbox of the program MATLAB[®].

4. Numerical results

To show the model capability of reproducing the macroscopic behaviour of SMA materials, we perform a number of stress-driven numerical experiments, in particular uniaxial and biaxial tests. In all tests we consider the material properties specified in Table 1 and compatible with Cu-based alloys (see e.g. Refs. 27,28), where E and ν are respectively the Young's modulus and the Poisson's ratio, while all the other material constants have already been introduced in Sec. 2.

Uniaxial tests represent the simplest setting on which it is possible to show the main features of the model as well as to appreciate the role played by the single material parameters; while biaxial tests allow to assess the model behaviour under complex non-proportional multi-axial loading conditions. All the numerical experiments have been performed in both the

Table 1. Material parameters.

parameter	value	unit
E	$5 \cdot 10^4$	MPa
ν	0.35	-
β	2	MPa K ⁻¹
M_f	223	K
h	1000	MPa
R	50	MPa
ε_L	4	%
δ	10^{-8}	-

pseudo-elastic and the shape-memory regimes, but for brevity we report here only the most significative examples.

4.1. Uniaxial tests

To begin with, we consider the following uniaxial tests in the pseudo-elastic regime

- single and multiple tension cycles with permanent inelasticity,
- multiple tension cycles followed by multiple compression cycles with saturating permanent inelasticity,
- multiple tension cycles with saturating permanent inelasticity, including degradation effect.

On the other hand, in the shape-memory regime we consider

- multiple tension cycles at $T = M_f$, each one followed by heating strain recovery.

For each experiment, we plot the output axial stress–axial strain curve.

- Single and multiple tension cycles with permanent inelasticity. The first considered uniaxial test consists in studying the response of the model under tension cycles reaching a maximum axial stress of $\sigma_{max} = 300$ MPa. The numerical experiments are performed at a temperature $T = 298$ K and using the following model parameters: $H = 0$ MPa, $A = 0$ MPa and $\kappa = 2\%$. The choice of a non-zero parameter κ gives rise to a permanent inelasticity phenomenon, as shown by the axial stress–axial strain curves of Fig. 2, referring, respectively, to one and ten tension cycles.
- Multiple tension cycles followed by multiple compression cycles with saturating permanent inelasticity.

The goal of this test is to show the saturation of the permanent inelasticity. The experiment is performed at a temperature $T = 298$ K and using the following model parameters: $H = 1.5 \cdot 10^4$ MPa, $A = 0$ MPa and $\kappa = 2\%$. The left part of Fig. 3 shows the response to ten tension cycles. We note that, since H is different from zero, the permanent strain saturates and does not exceed the threshold (cf. Ref. 22)

$$\sqrt{2/3}\beta\langle T - M_f \rangle / H = \sqrt{2/3} \cdot 150 / (1.5 \cdot 10^4) = 0.816\%.$$

The right part of Fig. 3 reports the results when fifteen compression cycles follow the tension ones. Again, we can observe that permanent inelasticity is accumulated and saturates when reaching the same threshold as in the case of tension.

- Multiple tension cycles with saturating permanent inelasticity, including degradation effect.

We now want to investigate the effect induced on the model by the parameter A coupling the two internal variables. The experiment consists of fifteen tension loops performed at a temperature $T = 298$ K and using the following model parameters: $H = 1.5 \cdot 10^4$ MPa, $A = 2 \cdot 10^3$ MPa and $\kappa = 2\%$. As shown in Fig. 4, the choice of a non-zero value for A results in shifting down the loops. This sort of degradation effect is an important feature of the model as an analogous phenomenon is observed in experimental tests (see Fig. 1).

- Multiple tension cycles at $T = M_f$, each one followed by heating strain recovery.

The aim of this last uniaxial experiment is to study the behaviour of the model when reproducing the shape-memory effect. The input consists of ten cycles, each one constructed as a tension loop with a maximum stress $\sigma_{max} = 150$ MPa at a temperature $T = M_f$ followed by a heating process at a constant zero stress up to a temperature of 298 K. The left part of Fig. 5 refers to a test with $H = 0$ MPa, $A = 0$ MPa and $\kappa = 2\%$, while the right part refers to a test with $H = 1.5 \cdot 10^4$ MPa, $A = 2 \cdot 10^3$ MPa and $\kappa = 2\%$. Both of them show that an inelastic effect is activated, so that we observe only a partial shape recovery. We finally stress that in the first case, since $A = 0$ MPa, inelasticity is activated only during the heating process.

4.2. Biaxial tests

The goal of biaxial tests is to verify the behaviour of the model and its capability of reproducing permanent inelasticity when subjected to non-proportional multi-axial loading. Accordingly, we study the model response under the two following loading conditions

- non-proportional hourglass-shaped test,
- combined uniaxial tests.

For both of these numerical experiments, we report the stress input and the corresponding strain output plots.

- Non-proportional hourglass-shaped test.
The first considered biaxial test consists of a non-proportional test where σ_{11} and σ_{12} are led to $\sigma_{max} = 300$ MPa in the hourglass-shaped loading history of Fig. 6 (left), which is repeated five times. The experiment is performed at a temperature $T = 298$ K and using the following model parameters: $H = 1.5 \cdot 10^4$ MPa, $A = 4 \cdot 10^3$ MPa and $\kappa = 10\%$. The numerical results, reported in terms of first and fifth cycle in Fig. 6 (right), show that the new formulation proposed is capable of introducing and controlling permanent inelasticity effects even in non-proportional multi-axial tests.
- Ten tension cycles in direction 1 followed by twenty tension cycles in direction 2.

This last numerical experiment aims at showing the model response under loading conditions changing in their direction of application. It consists of uniaxial tension cycles whose direction is suddenly rotated of $\pi/2$ and is performed at a temperature $T = 298$ K using the following model parameters: $H = 1.5 \cdot 10^4$ MPa, $A = 0$ MPa and $\kappa = 2\%$. Figure 7 shows the axial stress–axial strain curves for the two loading directions. The numerical results prove the capability of the model of reproducing the features shown in uniaxial tests even under multi-axial loading conditions.

5. Conclusions

The present work discusses the 3D constitutive model for describing the macroscopic behaviour of SMA proposed in Refs. 21,22. With respect to the previous model presented in Ref. 13, this new one is able to describe SMA macroscopic behaviours taking into account also permanent inelasticity effects. Such effects can be introduced both with a saturating or a non-

saturation evolution. Moreover, also degradation can be included. Many numerical experiments have been presented in order to show and assess the model performance both in uniaxial and non-proportional multi-axial problems.

Acknowledgements

This work has been partially supported by the European Project HPRN-CT-2002-00284 “New Materials, Adaptive Systems and their Nonlinearities. Modelling, Control and Numerical Simulation”.

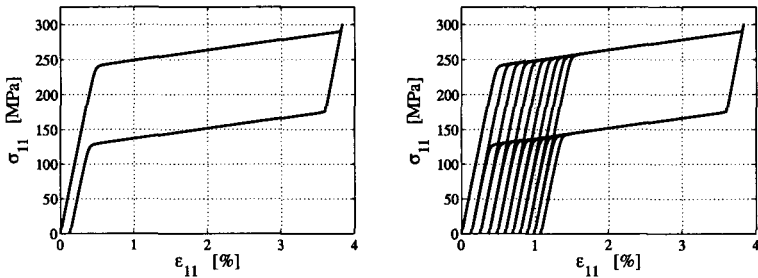


Fig. 2. Uniaxial tests: tension cycles with permanent inelasticity ($H = 0$ MPa, $A = 0$ MPa, $\kappa = 2\%$, $T=298K$). Axial stress–axial strain output for single (left) and multiple (right) tension loops.

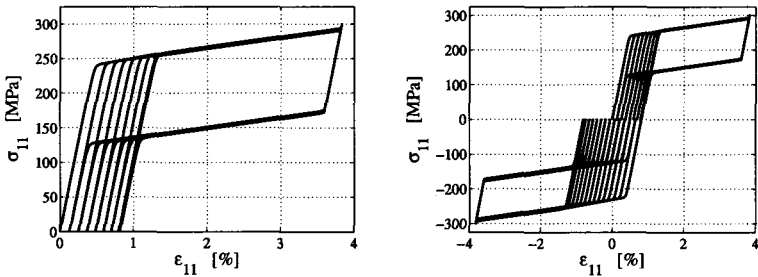


Fig. 3. Uniaxial tests: ten tension cycles (left) and ten tension followed by fifteen compression cycles (right) with saturating permanent inelasticity ($H = 1.5 \cdot 10^4$ MPa, $A = 0$ MPa, $\kappa = 2\%$, $T=298K$). Axial stress–axial strain output.

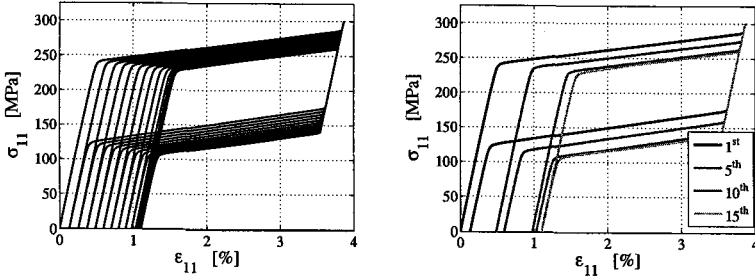


Fig. 4. Uniaxial tests: fifteen tension cycles with saturating permanent inelasticity, including degradation effect ($H = 1.5 \cdot 10^4$ MPa, $A = 2 \cdot 10^3$ MPa, $\kappa = 2\%$, $T = 298$ K). Axial stress–axial strain output.

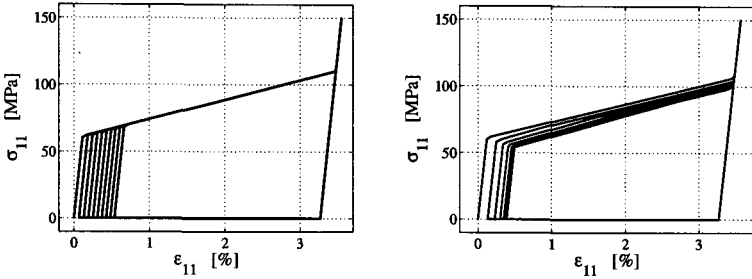


Fig. 5. Uniaxial tests: multiple (ten) tension cycles at $T = M_f$, each one followed by heating strain recovery, with $H = 0$ MPa, $A = 0$ MPa (left) and $H = 1.5 \cdot 10^4$ MPa, $A = 2 \cdot 10^3$ MPa (right) and $\kappa = 2\%$. Axial stress–axial strain output.

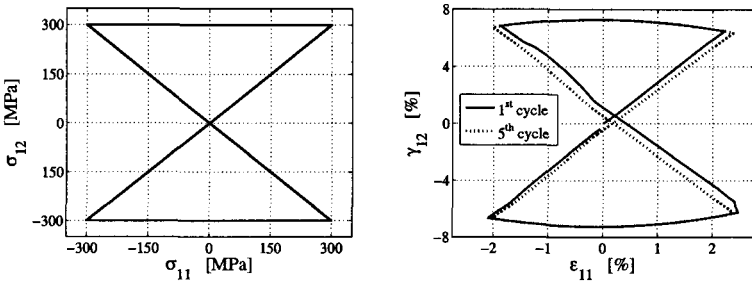


Fig. 6. Biaxial tests: non-proportional hourglass-shaped test ($H = 1.5 \cdot 10^4$ MPa, $A = 4 \cdot 10^3$ MPa, $\kappa = 10\%$, $T = 298$ K). $\sigma_{11} - \sigma_{12}$ input (left) and 1st and 5th cycle $\epsilon_{11} - \gamma_{12}$ output (right).

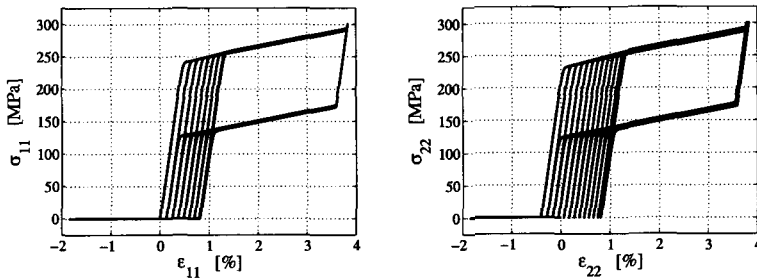


Fig. 7. Combined uniaxial tests: ten tension cycles in direction 1 followed by twenty in direction 2 ($H = 1.5 \cdot 10^4$ MPa, $A = 0$ MPa, $\kappa = 2\%$, $T = 298$ K). $\sigma_{11} - \varepsilon_{11}$ output (left) and $\sigma_{22} - \varepsilon_{22}$ output (right).

References

1. T. Duerig and A. Pelton (eds.), *SMST-2003 Proceedings of the International Conference on Shape Memory and Superelastic Technology Conference* (ASM International, 2003).
2. T. W. Duerig, K. N. Melton, D. Stoekel and C. M. Wayman, *Engineering aspects of shape memory alloys* (Butterworth-Heinemann, London, 1990).
3. C. Bouvet, S. Calloch and C. LExcellent, *European Journal of Mechanics A/Solids* **23**, 37–61 (2004).
4. S. Govindjee and C. Miehe, *Computer Methods in Applied Mechanics and Engineering* **191**, 215–238 (2001).
5. D. Helm and P. Haupt, *International Journal of Solids and Structures* **40**, 827–849 (2003).
6. S. Leclercq and C. LExcellent, *Journal of Mechanics and Physics of Solids* **44**, 953–980 (1996).
7. V. I. Levitas, *International Journal of Solids and Structures* **35**, 889–940 (1998).
8. V. I. Levitas, and D. L. Preston, *Physical Review B* **66**, 134206:1–9 (2002).
9. V. I. Levitas, and D. L. Preston, *Physical Review B* **66**, 134207:1–15 (2002).
10. B. Peultier, T. Benzineb and E. Patoor, *Journal de Physique IV France* **115**, 351–359 (2004).
11. B. Raniecki and C. LExcellent, *European Journal of Mechanics, A: Solids* **13**, 21–50 (1994).
12. A. C. Souza, E. N. Mamiya and N. Zouain, *European Journal of Mechanics, A: Solids* **17**, 789–806 (1998).
13. F. Auricchio and L. Petrini, *International Journal for Numerical Methods in Engineering* **61**, 807–836 (2004).
14. M. Arrigoni, F. Auricchio, V. Cacciafesta, L. Petrini and R. Pietrabissa, *Journal de Physique IV France* **11**, 577–582 (2001).
15. H. Funakubo (ed.), *Shape Memory Alloys* (Gordon and Breach Science Publishers, New York, 1987).

16. K. Otsuka and C. M. Wayman (eds.), *Shape Memory Materials* (Cambridge University Press, 1998).
17. Z. Bo and D. C. Lagoudas, D. C., *International Journal of Engineering Science* **37**, 1175–1203 (1999).
18. S. Govindjee and E. P. Kasper, *Journal for Intelligent Material Systems and Structures* **8**, 815–823 (1997).
19. D. C. Lagoudas and P. Entchev, *Mechanics of Materials* **36**, 865–892 (2004).
20. A. Paiva, M. A. Savi, A. M. B. Braga and P. M. C. L. Pacheco, *International Journal of Solids and Structures* **42**, 3439–3457 (2005).
21. F. Auricchio and A. Reali, *Mechanics of Advanced Materials and Structures* **14**, 43–55 (2007).
22. F. Auricchio, A. Reali and U. Stefanelli, A three-dimensional model describing stress-induced solid phase transformation with permanent inelasticity, *International Journal of Plasticity*, available online (2007).
23. F. Auricchio and L. Petrini, *International Journal for Numerical Methods in Engineering* **61**, 716–737 (2004).
24. F. Auricchio, A. Reali and U. Stefanelli, Analysis of a model describing stress-induced solid phase transformation with permanent inelasticity, in preparation (2006).
25. F. Auricchio, A. Mielke and U. Stefanelli, A rate-independent model for the evolution of shape memory materials, in preparation (2006).
26. J. C. Simo and T. J. R. Hughes, *Computational Inelasticity* (Springer-Verlag, New York, 1998).
27. P. Šittner, Y. Hara and M. Tokuda, *Metallurgical and Materials Transactions* **26A**, 2923–2935 (1995).
28. P. Šittner and V. Novák, *International Journal of Plasticity* **16**, 1243–1268 (2000).